ISSN 0016-7932, Geomagnetism and Aeronomy, 2018, Vol. 58, No. 2, pp. 281–289. © Pleiades Publishing, Ltd., 2018.
Original Russian Text © A.V. Koval, N.M. Gavrilov, A.I. Pogoreltsev, N.O. Shevchuk, 2018, published in Geomagnetizm i Aeronomiya, 2018, Vol. 58, No. 2, pp. 295–303.

Propagation of Stationary Planetary Waves in the Upper Atmosphere under Different Solar Activity

A. V. Koval[a, *], N. M. Gavrilov[a], A. I. Pogoreltsev[a, b], and N. O. Shevchuk[a]

[a]*St. Petersburg State University, St. Petersburg, 199034 Russia*
[b]*Russian State Hydrometeorological University, St. Petersburg, 195196 Russia*
**e-mail: a.v.koval@spbu.ru*

Received March 16, 2017; in final form, May 12, 2017

Abstract—Numerical modeling of changes in the zonal circulation and amplitudes of stationary planetary waves are performed with an accounting for the impact of solar activity variations on the thermosphere. A thermospheric version of the Middle/Upper Atmosphere Model (MUAM) is used to calculate the circulation in the middle and upper atmosphere at altitudes up to 300 km from the Earth's surface. Different values of the solar radio emission flux in the thermosphere are specified at a wavelength of 10.7 cm to take into account the solar activity variations. The ionospheric conductivities and their variations in latitude, longitude, and time are taken into account. The calculations are done for the January—February period and the conditions of low, medium, and high solar activity. It was shown that, during high-activity periods, the zonal wind velocities increases at altitudes exceeding 150 km and decreases in the lower layers. The amplitudes of planetary waves at high solar activity with respect to the altitude above 120 km or below 100 km, respectively, are smaller or larger than those at low activity. These differences correspond to the calculated changes in the refractive index of the atmosphere for stationary planetary waves and the Eliassen—Palm flux. Changes in the conditions for the propagation and reflection of stationary planetary waves in the thermosphere may influence the variations in their amplitudes and the atmospheric circulation, including the lower altitudes of the middle atmosphere.

DOI: 10.1134/S001679321802010X

1. INTRODUCTION

Large-scale wave disturbances play an important role in formation the general circulation, temperature regime, and composition of the middle and upper atmosphere (Holton, 1975). Due to the rapid progress in computer engineering and the improvement of numerical models of the general atmospheric circulation, there has recently been an upsurge in interest in the study of dynamical and thermal effects produced by wave motions, particularly, planetary waves (PWs), in different atmospheric layers. According to Haynes et al. (1991), the wave disturbances in the upper mesosphere and thermosphere is a key driving force that influences the extratropical circulation of the atmosphere.

The reflection of PWs in the middle and upper atmosphere can exert a considerable influence on atmospheric circulation (e.g., Lu et al., 2017). Substantial gradients of the temperature and wind in the thermosphere may be one of the causes of PW reflection in the upper atmosphere. The incoming solar radiation and heating depend on solar activity (SA), which experiences cyclical changes with a period of about 11 years (e.g., Vitinskii, 1986). SA variations can influence the temperature and circulation by changing the conditions for PW propagation and reflection in the upper atmosphere (Geller and Alpert, 1980; Arnold and Robinson, 1998).

Remote measurements of the temperature at the mesopause altitudes in 1980—2007 revealed the presence of PWs with periods of 2—10 days correlating with the 22-year Hale cycle (Hoppner and Bittner, 2007). In an analysis of long-term observations of the wind velocity at altitudes of the mesosphere and lower thermosphere (MLT), a positive correlation was found between the solar flux changes and the activity of planetary waves with periods of 3 to 20 days (Jacobi et al., 2008). Krivolutskii et al. (2015) modeled the influence of SA cyclicity on changes in the temperature and zonal wind at altitudes from 0 up to 135 km. They showed that PWs play an important role, connecting the upper atmosphere with the underlying layers. Chanin (2006) compared the data of measurements and numerical calculations covering a 45-year period and showed that the SA variations in the upper atmospheric layers significantly influence the propagation of PWs, which may redistribute the incoming solar energy. Jarvis (2006) analyzed the geomagnetic data for the Northern Hemisphere obtained during eight 11-year solar cycles in the 20th century; he found the 22-year modulation of a 5-day PW with changes in wave activity up to 20% at the altitudes of the mesosphere and lower thermosphere.

In most numerical models used to estimate the propagation and reflection of thermospheric PWs , the upper boundaries were at altitudes below 150 km. This does not allow temperature and circulation changes, which may cover large altitudes in the thermosphere, to be completely taken into account. Pogoreltsev et al. (2007) developed a thermospheric version of the Middle/Upper Atmosphere Model (MUAM) to calculate the general atmospheric circulation and PWs in an altitude range from the Earth's surface up to 300 km. Here, we use this model to study the propagation and reflection of stationary planetary waves (SPWs) under the variable impact of SA on the thermosphere.

In addition to the impact on the thermosphere, SA may directly influence the underlying atmospheric layers. For example, the flux of galactic cosmic rays, which anticorrelate with the incoming solar radiation, may result in anticovariation between the global cloudiness and the incoming solar radiation in the troposphere/stratosphere (Pudovkin and Veretenenko, 1995). In order to consider the effect of the thermosphere alone, the SA changes are specified here only at the altitudes above 100 km. For the lower altitudes, all of the calculations use the same conditions corresponding to the mean SA level. In parallel with the analysis of the effect of changes in the thermospheric temperature and circulation on the SPW propagation, the specified formulation of the problem makes it possible to estimate how strongly the thermospheric changes may influence the circulation and thermal regime in the underlying regions of the middle atmosphere during the SA variations.

2. GENERAL CIRCULATION MODEL COUPLED WITH MUAM

To analyze the influence of SA on SPW characteristics, numerical experiments with the use of the MUAM (Pogoreltsev et al., 2007) have been performed. At the lower boundary, the SPW amplitudes are specified on the basis of the geopotential heights in the lower atmospheric layers taken from the database of the Japanese 55-year Reanalysis of meteorological information (JRA-55) (Kobayashi et al., 2015) for January and averaged over 2005–2014. Different MUAM versions were described in papers by Gavrilov et al. (2013, 2014, 2015) and Koval et al. (2015), in which the dynamical and thermal impact of orographic gravity waves on the general circulation of the atmosphere, quasi-biennial oscillations, and PWs were studied. In the used MUAM version, the horizontal grid has 36 by 64 points in latitude and longitude, respectively. The vertical grid has 56 levels corresponding to the altitudes from the Earth's surface up to 300 km. Koval et al. (2015) describe the procedure that initializes the MUAM.

The radiation unit of the MUAM takes into account the dependence of solar radiation on SA, which is indicated by the radio emission flux from the Sun at a wavelength of 10.7 cm ($F10.7$). The flux $F10.7$ is characterized by the cyclicity with a period of the main 11-year SA cycle (Bruevich and Yakunina, 2015). In this study, we analyzed the time series of observations of $F10.7$ for the last six solar cycles (Royal Observatory of Belgium, 2013). To characterize low, medium, and high levels of SA, we selected the $F10.7$ values at 70, 130, and 220 sfu, respectively (1 sfu = 10^{-22} W/(m^2 Hz)). Since the objective of this paper is to analyze the SA impact on the thermosphere (see above), different values of $F10.7$ were specified only above the 100-km level in the radiation and thermospheric units of the MUAM. Below 100 km, the constant value of $F10.7$ = 130 sfu, which corresponds to the mean SA level, was used in all of the calculations.

To consider the influence of charged particles on the motion of neutral gas at the ionospheric altitudes, the ionospheric conductivities are specified in the MUAM and their variability with latitude, longitude, and time is taken into account. The magnetic torque and ion friction were determined by formulas

$$M = \frac{\sigma_2 H_z H_0}{c^2}; \quad I = -\frac{\sigma_1 H_0^2}{\rho c^2}, \tag{1}$$

respectively (Shevchuk and Pogoreltsev, 2016). Here, H_0 is the modulus of the magnetic strength vector, and H_z is its vertical component; c is the speed of light; ρ is the density of the neutral atmosphere; and σ_1 and σ_2 are the Pedersen and Hall ionospheric conductivities, respectively. The latter two are calculated with formulas

$$\sigma_1 = eN\left(\mu_1^{\mathrm{e}} + \mu_1^{\mathrm{i}}\right); \quad \sigma_2 = eN\left(\mu_2^{\mathrm{e}} - \mu_2^{\mathrm{i}}\right), \tag{2}$$

respectively (Pogoreltsev, 1996). Here, e and N are the electron charge and the number density of electrons, respectively. In these equations, the mobility of electrons and ions is determined by expressions

$$\begin{aligned}
\mu_1^{\mathrm{e}} &= \frac{e}{m_{\mathrm{e}} A \nu_{\mathrm{in}}^2}\left(\omega_{\mathrm{i}}^2 \nu_{\mathrm{en}} + \nu_{\mathrm{e}} \nu_{\mathrm{in}}^2\right); \\
\mu_1^{\mathrm{i}} &= \frac{e}{m_{\mathrm{i}} A \nu_{\mathrm{in}}}\left(\omega_{\mathrm{e}}^2 + \nu_{\mathrm{e}} \nu_{\mathrm{en}}^2\right); \\
\mu_2^{\mathrm{e}} &= \frac{e\omega_{\mathrm{e}}}{m_{\mathrm{e}} A \nu_{\mathrm{in}}^2}\left(\omega_{\mathrm{i}}^2 + \nu_{\mathrm{in}}^2 + \frac{m_{\mathrm{e}}}{m_{\mathrm{i}}} \nu_{\mathrm{ei}} \nu_{\mathrm{in}}\right); \\
\mu_2^{\mathrm{i}} &= \frac{e\omega_{\mathrm{e}}}{m_{\mathrm{e}} A \nu_{\mathrm{in}}^2}\left(\omega_{\mathrm{i}}^2 + \frac{m_{\mathrm{e}}}{m_{\mathrm{i}}} \nu_{\mathrm{ei}} \nu_{\mathrm{in}}\right),
\end{aligned} \tag{3}$$

respectively, (Gurevich and Tsedilina, 1967). Here, m_{e} and m_{i} are the electron mass and the mean mass of ions, respectively; ω_{e} and ω_{i} are the cyclotron (Larmor) frequency for electrons and ions, respectively; and ν_{ei}, ν_{en}, and ν_{in} are the collision frequencies for electrons and ions, electrons and neutral particles, and ions and neutral particles, respectively. Calculations according to formulas (1)–(3) were done with the ionospheric parameters taken from the semiempirical models of the neutral atmosphere NRL-MSISE and ionosphere IRI-Plas (Shevchuk and Pogoreltsev, 2016). The zonal averages of the magnetic torque and ion friction were calculated with formulas (1)–(3) for January with taking into account diurnal variations for all of the latitudes, longitudes, and 23 vertical levels above 100 km and incorporated into the MUAM.

One of the input parameters for the NRL-MSISE and IRI-Plas models is the flux $F10.7$, which makes it possible to take into account the dependence of the atmospheric and ionospheric characteristics on the SA variations, if the flux values $F10.7 = 70$ and 220 are specified for the low and high SA levels, respectively. Thus, the dependence of the modeled ionospheric conductivities on SA in the MUAM is determined by the dependence of the parameters required to calculate the conductivities (i.e., the electron concentration, the composition of the neutral and ionized components, etc.) on SA.

To interpret the model results, we calculated the latitude–altitude distributions of the quasi-geostrophic zonal mean complex refractive index squared (Karoly and Hoskins, 1982; Albers et al., 2013; Gavrilov et al., 2015)

$$n_m^2(\varphi, z) = \frac{\overline{q}_\varphi}{\overline{u} - c} - \left(\frac{m}{a\cos\varphi}\right)^2 - \left(\frac{f}{2NH}\right)^2, \qquad (4)$$

where $\overline{q}_\varphi$ is the latitudinal gradient of the zonal mean potential vorticity, $\overline{u}$ is the zonally averaged zonal wind velocity, $c = 2\pi a\cos\varphi/(m\tau)$ is the zonal phase velocity, τ is the wave period, φ and z is the latitude and altitude, respectively, a is the Earth's radius, f is the Coriolis parameter, N is the Brunt–Väisälä frequency, and H is the scale height of the atmosphere. According to Dickinson (1968) and Matsuno (1970), PWs propagate in the atmospheric regions where $n_m^2(\varphi, z) > 0$. These regions may be considered as waveguides of PWs. The structures of these waveguides are presented in section 3.3.

It is commonly supposed that another characteristic of PWs is the Eliassen–Palm flux vector (the EP flux) $F_m = (F_m^{(\varphi)}, F_m^{(z)})$.

For quasi-geostrophic conditions and a log-isobaric vertical coordinate, the corresponding components of the EP flux (divided by the density) can be expressed in the following form (Andrews et al., 1987)

$$F_m^{(\varphi)} = -a\cos\varphi(\overline{u'v'}), \quad F_m^{(z)} = af\cos\varphi(\overline{v'\theta'})/\overline{\theta}_z, \quad (5)$$

where primes indicate the disturbances induced by the considered PW modes. According to formula (5), the upward EP flux corresponds to the northward wave heat flux of SPWs, while the southward EP flux corresponds to the northward momentum flux of SPWs. The EP flux divergence determines the zonal mean flow acceleration produced by PWs.

3. MODEL RESULTS

In numerical experiments with the MUAM, to take into account the impact of the SA variations only in the thermosphere, we specified SA at a constant mean level below the altitude of 100 km, while the SA level above 100 km was changed from low to high (see section 2). We analyzed the changes in the general circulation of the atmosphere and the SPW amplitudes with the zonal wave numbers $m = 1$ and 2 (hereinafter referred to as SPW1 and SPW2, respectively) caused by the influence of SA on the thermosphere.

3.1. General Circulation of the Atmosphere

Figure 1a presents the altitude–latitude distributions of the longitude-mean zonal wind velocity averaged over the January–February period for high (left panel) and low (middle panel) SA and the corresponding increments of the zonal wind due to the SA increase (right panel). The general structure of the zonal circulation displayed in Fig. 1a is consistent with empirical models (e.g., Jacobi et al., 2009).

The right plot in Fig. 1a shows that, at midlatitudes of the Northern Hemisphere at altitudes above 160 km, the zonal wind velocity is larger (by 60–80%) for high SA than that for low SA. In the Southern Hemisphere, the dependence is opposite. As it is seen in Fig. 1a (right), below the 160-km level, the regions of positive and negative increments of zonal wind alternate. The relative increments of the zonal velocity values at altitudes of 90–120 km may reach 25%. An interesting feature is the region at high latitudes of the Northern Hemisphere at altitudes of 30–60 km, where the zonal wind velocity substantially decreases with growing SA (see Fig, 1a, right panel). This means that the effect produced by SA in the thermosphere may considerably influence the general circulation of the middle atmosphere.

The changes in the zonal wind velocity seen in Fig. 1a can be explained by the SA influence on the meridional gradients of the temperature. The left and middle plots of Fig. 1b show the longitude-mean meridional temperature gradients averaged over the January–February period for high and low SA, respectively, while their increments are in the right plot of Fig. 1b. According to the theory, the thermal component of the zonal wind is proportional to the mean meridional temperature gradient, while a positive gradient of the temperature in the Northern Hemisphere corresponds to the decrease in the wind velocity (e.g., Gill, 1982). This theory is confirmed by a comparison of the panels on the right side of Fig. 1, where the negative increments of the meridional temperature gradient in the Northern Hemisphere mainly correspond to positive increments of the zonal velocity and vice versa. In the

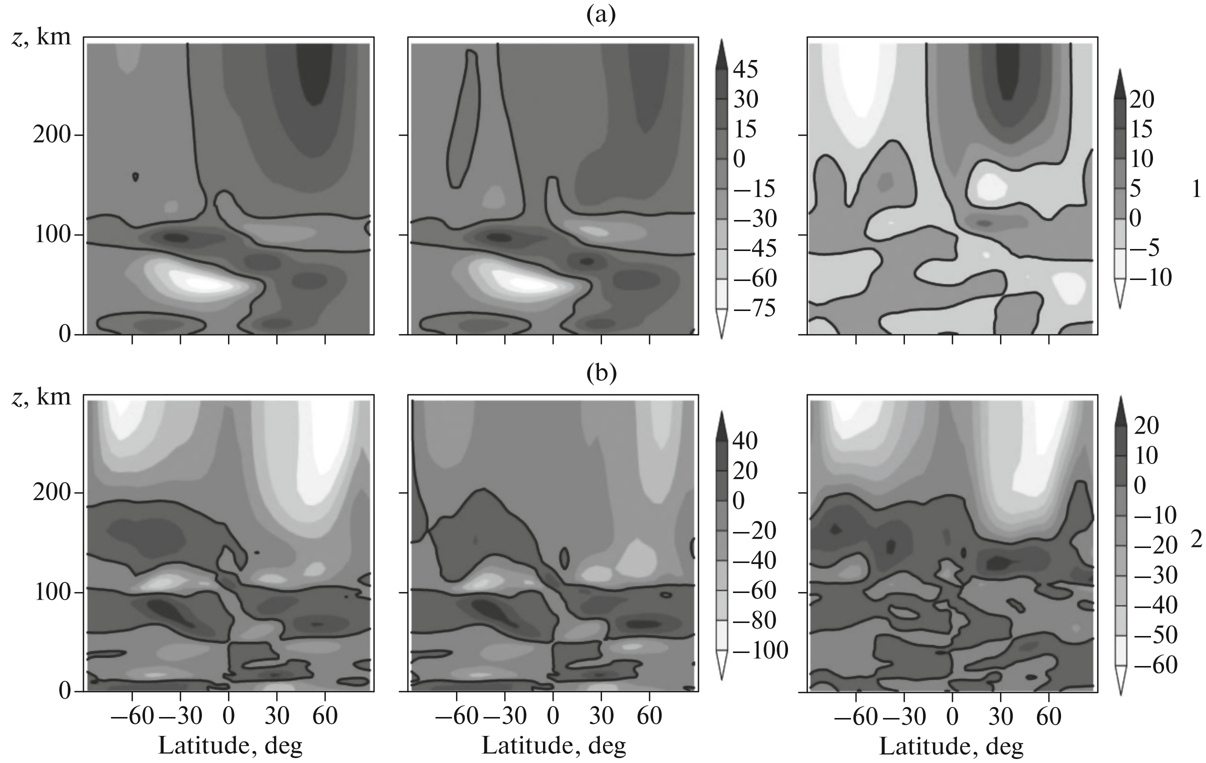

Fig. 1. Distributions of the longitude-mean zonal wind velocity (expressed in m/s) (a) and the meridional temperature gradient (expressed in K/deg) (b) under high (left panels) and low (middle panels) SA; the corresponding increments due to the SA increase are in the right panels. The quantities are averaged over the January–February period.

Southern Hemisphere, the signs of increments of the meridional temperature gradient and the zonal velocity mainly coincide (right panels of Fig. 1).

Analysis of the different heat inflows contributing to the MUAM equation for the temperature shows that the solar heating at high altitudes in the thermosphere is largest at high latitudes of the summer (Southern) Hemisphere and is smallest at high latitudes of the winter (Northern) Hemisphere. Because of this, negative meridional gradients of the temperature are prevalent above 200 km (see Fig. 1b). Dynamical processes and atmospheric circulation produce additional heat inflows, which are mainly dominated by horizontal temperature advection and adiabatic changes of temperature during vertical motions of air. The plot on the right plot in Fig. 1b shows that, due to the increase in SA, the absolute value of the negative meridional gradients of the temperature increases in the thermosphere above 200 km and decreases at altitudes of 120–180 km. This produces the corresponding changes in the mean zonal wind velocity (see Fig. 1a, right panel).

In the described models, the influence of SA on solar heat inflows was taken into account only above 100 km. Consequently, the increments of the meridional temperature gradients below 100 km (see Fig. 1b, right panel) are caused by changes in the dynamical heat inflows mentioned above and reflect the changes in atmospheric circulation below 100 km (see Fig. 1a, right panel) connected with the impact of SA on the thermosphere. Such changes can be induced by the varying conditions for PW reflections in the thermosphere during SA variations, which are considered below.

3.2. SPW Amplitudes

Figures 2a and 2b present the altitude–latitude distributions of the amplitudes of SPW1 and SPW2 with zonal wave numbers $m = 1$ and 2, respectively, in the geopotential fields; the quantities are averaged over the January–February period. The left and middle panels in Fig. 2 correspond to the high and low SA levels, while the SPW amplitude increments caused by the SA increase are in the right panels. As is seen, at altitudes below 90 km, the SPW amplitudes are larger at mid- and high latitudes of the Northern Hemisphere, which is explained by the eastward atmospheric circulation in the winter stratosphere/mesosphere. In the middle atmosphere of the Southern Hemisphere, the zonal circulation direction changes with altitude (see Fig. 1a), which produces barriers to SPW propagation at altitudes where the wind changes its sign (Charney and Drazin, 1961). The SPW amplitudes obtained for altitudes below 60 km were com-

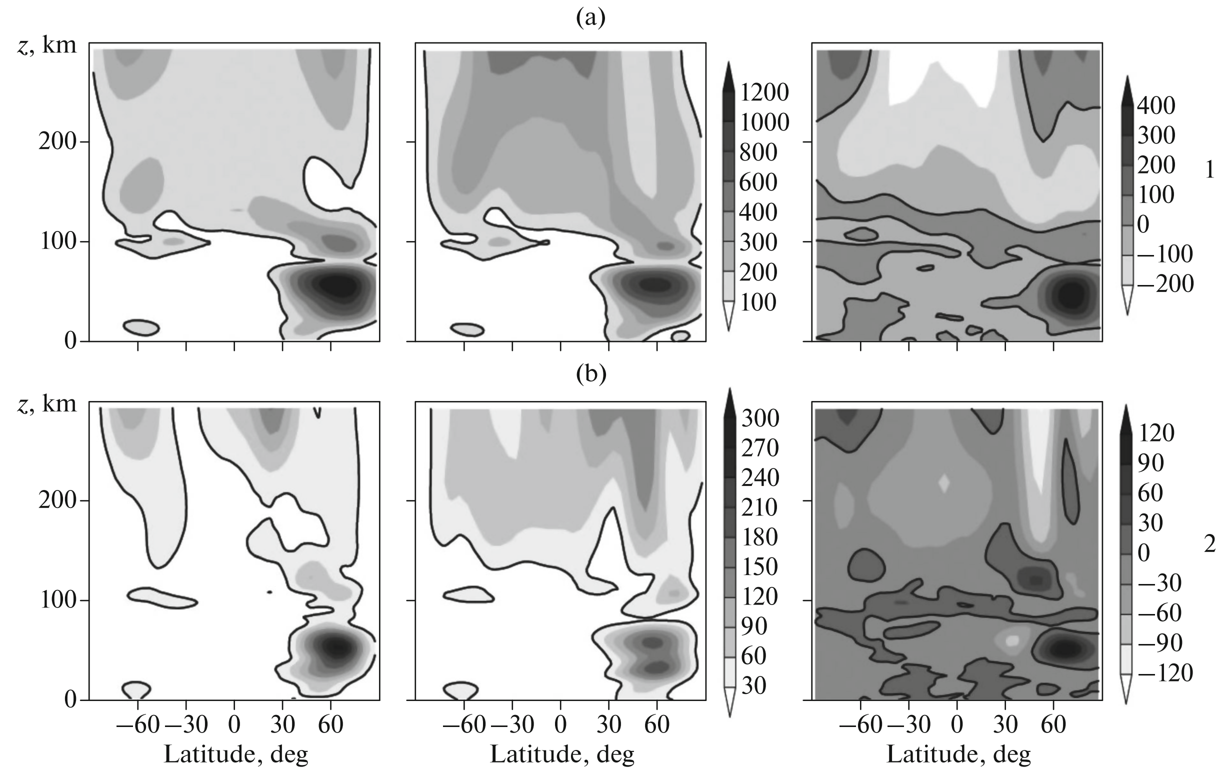

Fig. 2. Distributions of the amplitudes of geopotential variations (expressed in geopotential meters (gpm)) induced by SPW1 (a) and SPW2 (b) under high (left panel) and low (middle panel) SA; the increments of the SPW amplitudes due to the SA increase are in the right panels. The quantities are averaged over the January–February period.

pared to the UK Met Office data on the assimilation of meteorological information about the troposphere/stratosphere (Swinbank and O'Neill, 1994). We found that the SPW1 and SPW2 amplitudes calculated with the MUAM and obtained from the assimilation agree well.

At altitudes above 100 km, the SPW1 and SPW2 amplitudes are considerable in both hemispheres. This is explained by the larger latitudinal extension of the waveguide for SPWs in the thermosphere (see below). Figure 2 shows that, above 120–150 km in the thermosphere of the both hemispheres, the SPW1 and SPW2 amplitudes are mainly smaller at high SA than those at low SA. From the right panels of Fig. 2, it is seen that, at altitudes of 30–70 km, the SPW1 and SPW2 amplitudes at high latitudes of the Northern Hemisphere substantially increase (up to 30–40%) with increasing SA from a low level to a high one. This corresponds to the region of the decrease in the zonal wind velocity noticed earlier in the right plot of Fig. 1a. In the literature, the change in the conditions for the reflection of PW energy at high altitudes during SA variations is considered to be one of the probable mechanisms of SA impact on the dynamics of the middle atmosphere (Arnold and Robinson, 1998; Lu et al., 2017). Figure 2 shows that SPWs propagating from the underlying atmosphere are reflected at a lower boundary of the thermosphere to a lesser degree when SA is low than when it is high. Because of this, the SPW amplitudes in Fig. 2 are larger in the thermosphere and smaller in the middle atmosphere under low SA than those under high SA. The conditions for propagating SPWs are characterized by the refractive index of the atmosphere for PWs and by the EP fluxes, which are analyzed below.

3.3. Refractive Index of PWs and EP Fluxes

To interpret the modeled SPW amplitudes considered above, we calculated the refractive indices of the atmosphere for SPWs and EP fluxes (see section 2). They are displayed in Fig. 3 for high and low SA. As seen in the left and middle plots of Fig. 3, the waveguide regions (where $n_m^2(\varphi, z) > 0$ (see section 2)) at altitudes of 20–60 km are mainly in the Northern Hemisphere, in the zone of medium values of the eastward zonal velocity. Above 60–70 km, these zones cross the equator and reach the Southern Pole at altitudes of 90–120 km. In the thermosphere, the waveguides above 120 km cover the mid- and low latitudes of the Northern Hemisphere and may reach the midlatitudes of the Southern Hemisphere (see Fig. 3). The EP fluxes in Fig. 3 are mainly directed along the mentioned waveguides. In Fig. 2, the nonzero amplitudes

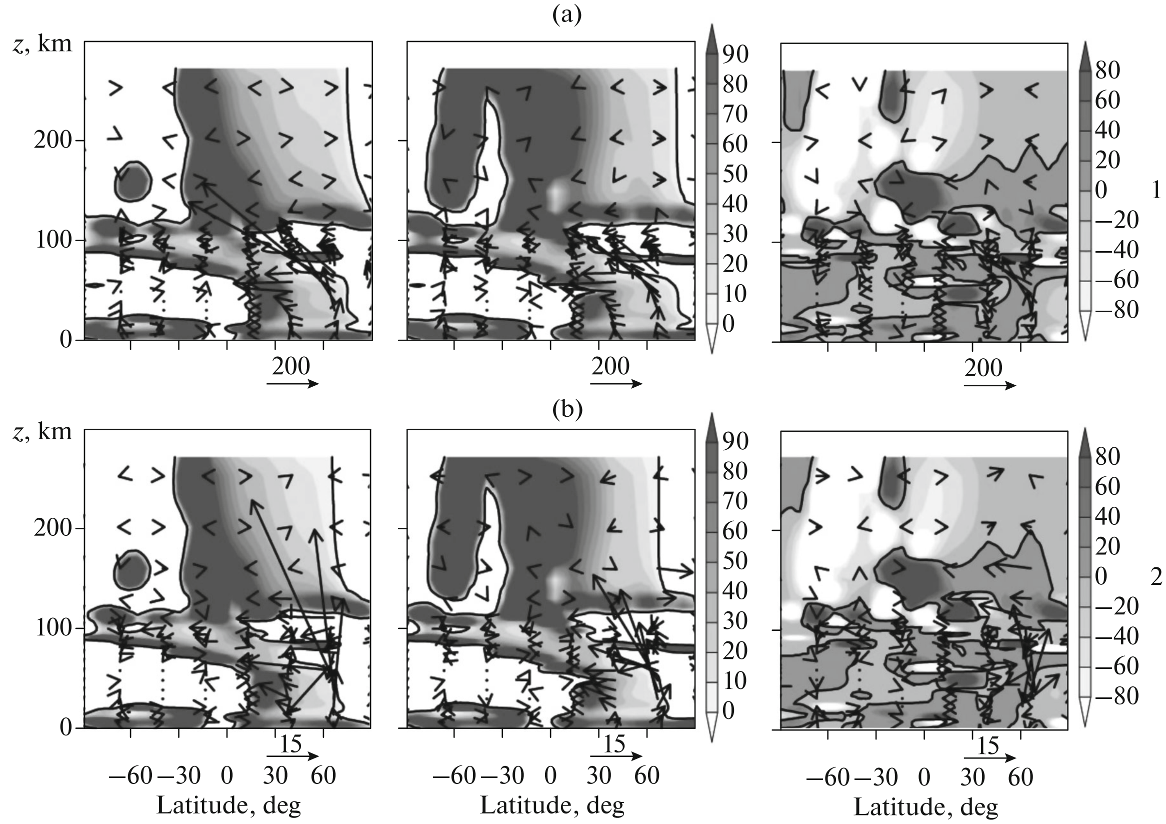

Fig. 3. Normalized squared refractive index of the atmosphere for SPWs (shaded) and the Eliassen–Palma flux vector (expressed in m^3/s^2) (arrows, the vertical component is multiplied by 100 for illustration purposes) for SPW1 (a) and SPW2 (b) under high (left panel) and low (middle panel) SA; the increments of these quantities due to the SA increase are in the right panels. The quantities are averaged over the January–February period.

of SPWs occur in the regions of the middle atmosphere located outside the waveguides. It is seen in Figs. 3a and 3b that some long vectors of the EP flux originate from the regions where $n_m^2(\varphi, z) < 0$. This probably means that the corresponding SPWs may be generated in the middle atmosphere due to, for example, nonlinear interaction of different wave harmonics with the mean flow.

The changes in the fields of the temperature and zonal velocity induced by SA variations yield changes in the configuration of waveguide zones (see left and middle panels in Fig. 3). In the thermosphere above 180 km, increased SA results in decreases in the refractive index (right panels in Fig. 3) and diminished penetration of the waveguide zone into the Southern Hemisphere (see middle panels in Fig. 3). The decrease in the refractive index and the northward vectors of the EP-flux increments (see Fig. 3) favor worse conditions for propagating SPWs in these regions of the thermosphere during high SA and the corresponding smaller amplitudes of SPWs in the left panels of Fig. 2.

The right panels of Fig. 3 show the negative changes of the squared refractive index at altitudes of 90–120 km at increased SA. At these altitudes, the worsening conditions for SPW propagation from the underlying layers may produce additional barriers for SPW penetration into the thermosphere and strengthen wave reflection at high SA. This is confirmed by Fig. 4, which presents the vertical component of the EP flux averaged over the January–February period. In the regions of maxima in the SPW1 and SPW2 amplitudes at altitudes of 50–70 km at mid- and high latitudes of the Northern Hemisphere seen in Fig. 2, significant upwelling EP fluxes, especially during high SA, are observed in the corresponding plots of Fig. 4. These fluxes may favor the formation of maxima in the SPW amplitudes at these altitudes. The vertical EP flux for SPW1 decays more rapidly under high SA and becomes weaker at altitudes of 90–110 km than that under low SA (see the corresponding negative increments of the EP flux in the right panels of Fig. 4a). This may indicate stronger reflection of PSW1 under high SA at the mentioned altitudes. This effect is more expressed for SPW2 in Fig. 4b, where the vertical EP flux changes its direction from upwell-

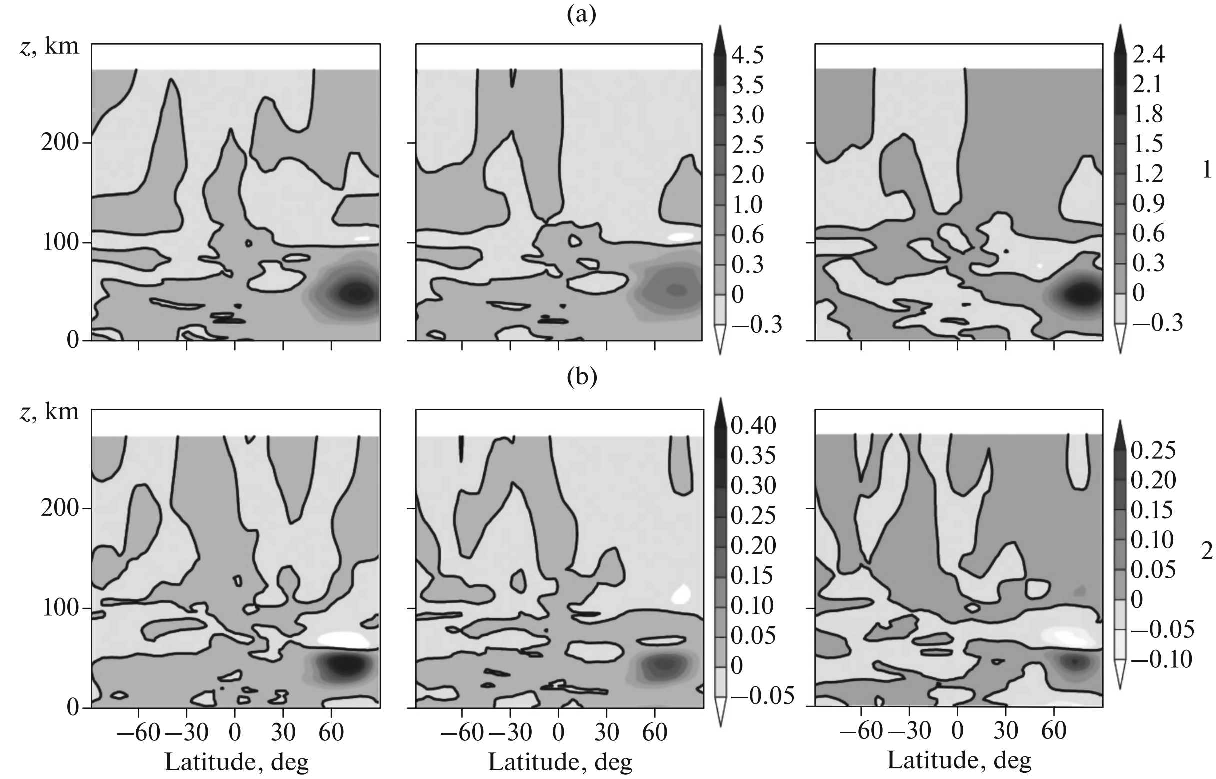

Fig. 4. Vertical component of the EP flux vector (expressed in m^3/s^2) for SPW1 (a) and SPW2 (b) under high (left panel) and low (middle panel) SA; the increments of these quantities due to the SA increase are in the right panels. The quantities are averaged over the January–February period.

ing to downwelling in the Northern Hemisphere at altitudes of 60–110 km due to the SA increase. Strengthening of the wave reflection may result in a decrease of the amplitudes of SPWs propagating into the thermosphere from the underlying atmosphere upon high SA.

According to the theory of SPWs (e.g., Andrews et al., 1987), the upward EP fluxes correspond to the northward wave flows of heat. Because of this, the substantial upwelling EP fluxes at high northern latitudes in the middle atmosphere (see Fig. 4) can intensively transfer heat to the Northern Pole and significantly warm the polar region during polar night. Such warming may diminish the velocity of the circumpolar vortex at high latitudes of the winter hemisphere. According to Fig. 4, the upwelling EP fluxes and the wave heating in the middle atmosphere is stronger at high SA. Thus, the strengthening of the wave heating in the polar region may contribute to the decrease of the mean zonal velocity at altitudes of 30–60 km at high latitudes of the Northern Hemisphere under increasing SA, which is noticeable in the right plot of Fig. 1a.

The described change in the reflection of SPWs in the upper atmosphere during in SA changes may partly explain the observed SA manifestations in the circulation of the middle atmosphere (see, e.g., Labitzke and van Loon, 1988). To analyze the SA-caused effects in the middle atmospheric layers in more detail, it is necessary to perform numerical modeling that takes into account not only SPW reflection in the thermosphere, but also the direct impacts of changes in solar radiation and intensity of cosmic rays on the thermal regime and dynamics of the middle atmosphere.

4. CONCLUSIONS

With the thermospheric version of the general circulation model of the atmosphere (MUAM), we calculated the amplitudes of SPWs with zonal wave numbers $m = 1$ and 2 for January–February at altitudes up to 300 km from the Earth's surface. For the thermosphere above 100 km, the SA variations were taken into account in calculations of the solar heating and ionospheric conductivities. The influence of SA on SPW propagation from the middle atmosphere to the thermospheric altitudes was studied.

Numerical experiments showed that the changes in temperature and circulation of the thermosphere under varying SA may substantially influence SPW propagation in the atmosphere. When SA is high, SPW amplitudes at altitudes above 120 km become smaller than those during low SA. These effects are explained by changes in the circulation of the atmosphere at different SA. In particular, substantial changes in the meridional gradients of the temperature lead to changes in the vertical profiles of the zonal wind, which influences SPW propagation.

In the Northern (winter) Hemisphere at altitudes below 100 km, the SPW amplitudes are larger (by 20–30%) at high SA than those at low SA. This may be connected with changes in the conditions of propagation and reflection of SPWs propagating from the troposphere at the altitudes of the thermosphere. To gain a better understanding of the propagation conditions for SPWs, we calculated the refractive indices and the EP fluxes corresponding to the considered SPWs. The stronger upwelling EP fluxes in the middle atmosphere of the Northern Hemisphere under high SA favor the increase of the SPW amplitudes at these altitudes. At altitudes of 60–110 km, the reflection of waves may become stronger, which weakens the upwelling EP flux for SPW1 and turns this flux to the downwelling one for SPW2 under high SA. The changes in the distributions of the squared refractive index and the EP fluxes at different levels of SA agree with the changes in the SPW amplitudes.

Our results show that the changes in the circulation and temperature regime of the thermosphere during the changes in SA may influence SPW propagation and reflection; moreover, the latter may induce noticeable changes of wind and temperature in the underlying atmospheric layers, including the middle atmosphere. Due to the increased reflection of waves in the thermosphere, the SPW amplitudes in the middle atmosphere of the Northern Hemisphere are larger during high SA than those under low SA conditions. In the middle atmosphere of the Southern Hemisphere, SPWs do not propagate because of the barriers appeared at the altitudes where the zonal wind changes its direction. At altitudes above 100 km, SPWs propagate along the waveguides in both the Northern and Southern Hemispheres. When this occurs, the SPW amplitudes above 120 km are larger during weak SA.

ACKNOWLEDGMENTS

The data on the magnetic swirling and ion friction were adapted and integrated for the MUAM under support of the Council on Grants of the President of the Russian Federation (MK-1424.2017.5). The calculations of SPWs, EP fluxes, and refractive indices were supported by the Russian Foundation for Basic Research (project no. 16-35-60013 mol_a_dk).

REFERENCES

Albers, J.R., McCormack, J.P., and Nathan, T.R., Stratospheric ozone and the morphology of the northern hemisphere planetary waveguide, *J. Geophys. Res.: Atmos.*, 2013, vol. 118, pp. 563–576. doi 10.1029/2012JD017937

Andrews, D.G., Holton, J.R., and Leovy, C.B., *Middle Atmosphere Dynamics*, New York: Academic, 1987.

Arnold, N.F. and Robinson, T.R., Solar cycle changes to planetary wave propagation and their influence on the middle atmosphere circulation, *Ann. Geophys.*, 1998, vol. 16, no. 1, pp. 69–76.

Bruevich, E.A. and Yakunina, G.V., The cyclic activity of the Sun from observations of the activity indices at different time scales, *Moscow Univ. Phys. Bull.*, 2015, vol. 70, no. 4, pp. 282–290. doi 10.3103/S0027134915040062

Chanin, M.-L., Signature of the 11-year cycle in the upper atmosphere, *Space Sci. Rev.*, 2006, vol. 125, pp. 261–272. doi 10.1007/s11214-006-9062-5

Charney, J.G. and Drazin, P.G., Propagation of planetary-scale disturbances from the lower into the upper atmosphere, *J. Geophys. Res.*, 1961, vol. 66, no. 1, pp. 83–109.

Dickinson, R.E., Planetary Rossby waves propagating vertically through weak westerly wave guides, *J. Atmos. Sci.*, vol. 25, pp. 984–1002.

Gavrilov, N.M., Koval, A.V., Pogoreltsev, A.I., and Savenkova, E.N., Numerical simulation of the response of general circulation of the middle atmosphere to spatial inhomogeneities of orographic waves, *Izv., Atmos. Ocean. Phys.*, 2013, vol. 49, no. 4, pp. 367–374.

Gavrilov, N.M., Koval, A.V., Pogoreltsev, A.I., and Savenkova, E.N., Numerical simulation of the influence of stationary mesoscale orographic waves on the meridional circulation and ozone fluxes in the middle atmosphere, *Geomagn. Aeron. (Engl. Transl.)*, 2014, vol. 54, no. 3, pp. 381–387.

Gavrilov, N.M., Koval, A.V., Pogoreltsev, A.I., and Savenkova, E.N., Simulating influences of QBO phases and orographic gravity wave forcing on planetary waves in the middle atmosphere, *Earth Planets Space*, 2015, vol. 67, no. 1. doi 10.1186/s40623-015-0259-2

Geller, M.A. and Alpert, J.C., Planetary wave coupling between the troposphere and the middle atmosphere as a possible Sun-weather mechanism, *J. Atmos. Sci.*, 1980, vol. 37, pp. 1197–1215.

Gill, A., *Atmosphere–Ocean Dynamics*, New York: Academic, 1982; Moscow: Mir, 1986.

Gurevich, A.V. and Tsedilina, E.E., Motion and spreading of inhomogeneities in a plasma, *Phys.-Usp.*, 1967, vol. 10, pp. 214–236.

Haynes, P.H., McIntyre, M.E., Shepherd, T.G., Marks, C.J., and Shine, K.P., On the "downward control" of extratropical diabatic circulations by eddy-induced mean zonal forces, *J. Atmos. Sci.*, 1991, vol. 48, no. 4, pp. 651–678.

Holton, J.R., *The Dynamic Meteorology of the Stratosphere and Mesosphere*, Boston: Am. Meteorol. Soc., 1975.

Hoppner, K. and Bittner, M., Evidence for solar signals in the mesopause temperature variability?, *J. Atmos. Sol.-Terr. Phys.*, 2007, vol. 69, pp. 431–448.

Jacobi, Ch., Hoffmann, P., and Kurschner, D., Trends in MLT region winds and planetary waves, Collm (52° N, 15° E), *Ann. Geophys.*, 2008, vol. 26, no. 5, pp. 1221–1232.

Jacobi, Ch., Fröhlich, K., and Portnyagin, Y., et al., Semi-empirical model of middle atmosphere wind from the ground to the lower thermosphere, *Adv. Space Res.*, 2009, vol. 43, pp. 239–246.

Jarvis, M.J., Planetary wave trends in the lower thermosphere—Evidence for 22-year solar modulation of the quasi 5-day wave, *J. Atmos. Sol.-Terr. Phys.*, 2006, vol. 68, no. 1, pp. 1902–1912.

Karoly, D.J. and Hoskins, B.J., Three dimensional propagation of planetary waves, *J. Meteorol. Soc. Jpn.*, 1982, vol. 60, no. 1, pp. 109–123.

Kobayashi, S., Ota, Y., and Harada, H., The JRA-55 reanalysis: General specifications and basic characteristics, *J. Meteorol. Soc. Jpn.*, 2015, vol. 93, no. 1, pp. 5–48. doi 10.2151/jmsj.2015-00

Koval, A.V., Gavrilov, N.M., Pogoreltsev, A.I., and Savenkova, E.N., Experiments on sensitivity of meridional circulation and ozone flux to parameterizations of orographic gravity waves and QBO phases in a general circulation model of the middle atmosphere, *Geosci. Model Dev. Discuss.*, 2015, vol. 8, no. 7, pp. 5643–5670. doi 10.5194/gmdd-8-5643-201

Krivolutsky, A.A., Cherepanova, L.A., Dement'eva, A.V., Repnev, A.I., and Klyuchnikova, A.V., Global circulation of the Earth's atmosphere at altitudes from 0 to 135 km simulated with the ARM model. Consideration of the solar activity contribution, *Geomagn. Aeron. (Engl. Transl.)*, 2015, vol. 55, no. 6, pp. 780–800.

Labitzke, K. and van Loon, H., Association between the 11-year solar cycle, the QBO, and the atmosphere. Part II: Surface and 700 mb in the northern hemisphere in winter, *J. Clim.*, 1988, vol. 1, no. 9, pp. 905–920.

Lu, H., Scaife, A.A., Marshall, G.J., Turner, J., and Gray, L.J., Downward wave reflection as a mechanism for the stratosphere–troposphere response to the 11-year solar cycle, *J. Clim.*, 2017, vol. 30, no. 7, pp. 2395–2414.

Matsuno, T., Vertical propagation of stationary planetary waves in the winter Northern Hemisphere, *J. Atmos. Sci.*, 1970, vol. 27, no. 6, pp. 871–883.

Pogoreltsev, A.I., Simulation of the influence of stationary planetary waves on the zonally averaged circulation of the mesosphere/lower thermosphere region, *J. Atmos. Terr. Phys.*, 1996, vol. 58, no. 10, pp. 1125–1141.

Pogoreltsev, A.I., Vlasov, A.A., Froehlich, K., and Jacobi, Ch., Planetary waves in coupling the lower and upper atmosphere, *J. Atmos. Sol.-Terr. Phys.*, 2007, vol. 69, no. 1, pp. 2083–2101.

Pudovkin, M.I. and Veretenenko, S.V., Cloudiness decreases associated with Forbush decreases of galactic cosmic rays, *J. Atmos. Sol.-Terr. Phys.*, 1995, vol. 57, no. 11, pp. 1349–1355.

Royal Observatory of Belgium (ROB), http://sidc.be/silso/datafiles.

Shevchuk, N.O. and Pogoreltsev, A.I., Upper atmosphere conductivity model and conductivities effects on modeling of atmospheric tides, in *Proc. Int. Conf. "Atmosphere, Ionosphere, Safety" (AIS-2016)*, Kaliningrad, 2016, p. 500.

Swinbank, R. and O'Neill, A., Stratosphere–troposphere assimilation system, *Mon. Weather Rev.*, 1994, vol. 122, pp. 686–702.

Vitinskii, Yu. I., Kopetskii, M., and Kuklin, G.V., *Statistika pyatnoobrazovatel'noi deyatel'nosti Solntsa* (Statistics of Solar Spot Generation Activity), Moscow: Nauka, 1986.

Translated by E. Petrova